HHS Public Access

Author manuscript

Nature. Author manuscript; available in PMC 2020 January 31.

Published in final edited form as:

Nature. 2019 August ; 572(7769): 397–401. doi:10.1038/s41586-019-1437-3.

Dietary methionine links nutrition and metabolism to the efficacy of cancer therapies

Xia Gao[1], **Sydney M. Sanderson**[1,¶], **Ziwei Dai**[1,¶], **Michael A. Reid**[1], **Daniel E. Cooper**[2], **Min Lu**[3,4], **John P. Richie Jr.**[5], **Amy Ciccarella**[6], **Ana Calcagnotto**[5], **Peter G. Mikhael**[1], **Samantha J. Mentch**[1], **Juan Liu**[1], **Gene Ables**[7], **David G. Kirsch**[1,2], **David S. Hsu**[3,4], **Sailendra N. Nichenametla**[7], **Jason W. Locasale**[1,*]

[1]Department of Pharmacology and Cancer Biology, Duke University School of Medicine, Durham, NC 27710, USA

[2]Department of Radiation Oncology, Duke University Medical Center, Durham, NC 27710, USA

[3]Center for Genomics and Computational Biology, Duke University, Durham, NC 27710, USA

[4]Department of Medical Oncology, Duke University Medical Center, Durham, NC 27710, USA

[5]Penn State University College of Medicine, Department of Public Health Sciences, Hershey, PA 17033, USA

[6]Penn State University Clinical Research Center, State College, PA 16802, USA

[7]Orentreich Foundation for the Advancement of Science, Cold Spring, NY 10516, USA

Summary

Nutrition exerts profound effects on health and dietary interventions are commonly used to treat diseases of metabolic etiology. Although cancer has a substantial metabolic component[1], the principles that define whether nutrition may be used to influence tumour outcome are unclear[2]. Nevertheless, it is established that targeting metabolic pathways with pharmacological agents or radiation can sometimes lead to controlled therapeutic outcomes. In contrast, whether specific dietary interventions could influence the metabolic pathways that are targeted in standard cancer therapies is not known. We now show that dietary restriction of methionine (MR), an essential amino acid, and the reduction of which has anti-aging and anti-obesogenic properties, influences cancer outcome through controlled and reproducible changes to one-carbon metabolism. This pathway metabolizes methionine and further is the target of a host of cancer interventions

*Correspondence: Jason Locasale – Jason.Locasale@duke.edu.

¶Equal contribution

AUTHOR CONTRIBUTIONS

X.G. and J.W.L. designed the study, X.G., and J.W.L. wrote and edited the paper. D.E.C. and D.G.K designed the sarcoma experiments and edited the paper. M.L. and D.S.H designed and implemented the colorectal PDX models and edited the paper. X.G., M.L, D.E.C., G.A., and M.A.R. performed animal experiments. X.G., S.M.S, and M.A.R performed all cell culture experiments. J.P.R., A.C., A.C., and S.N.N. conducted the human study. Z.D. conducted computational analyses with initial help from P.M. J.L., S.J.M. assisted in mass spectrometry metabolomics experiments.

CONFLICT OF INTEREST

J.W.L and X.G. have patents related to targeting amino acid metabolism in cancer therapy. D.G.K. is a co-founder and has equity in XRAD therapeutics, a company developing radiosensitizing agents. He also has patents related to radiosensitizing agents.

involving chemotherapy and radiation. MR produced therapeutic responses in chemoresistant RAS-driven colorectal cancer patient derived xenografts (PDXs) and autochthonous *KRAS*$^{G12D+/-}$;*TP53*$^{-/-}$ -driven soft tissue sarcomas resistant to radiation. Metabolomics revealed the therapeutic mechanisms to occur through tumour cell autonomous effects on the flux through one-carbon metabolism that impacted redox and nucleotide metabolism, thus interacting with the antimetabolite or radiation intervention. Finally, in a controlled and tolerated feeding study in humans, MR resulted in similar effects on systemic metabolism as obtained in responsive mice. These findings provide evidence that a targeted dietary manipulation can affect specific tumour cell metabolism to mediate broad aspects of cancer outcome.

Nutrient composition in growth media has dramatic effects on cancer cell metabolism [3–5]. However, the extent that diet through its influence on circulating metabolite levels, which is the corresponding situation *in vivo*, alters metabolic pathways in tumours and affects therapeutic outcomes is largely unknown. Studies have shown that the dietary removal of amino acids, serine and glycine, can modulate cancer outcome [6–8]. The availability of histidine and asparagine mediates the response to methotrexate [9] and the progression of breast cancer metastasis [10], respectively. Whether such interventions broadly affect metabolism or have targeted effects on specific pathways related to these nutrients is unknown. One intriguing possibility for a specific dietary intervention in cancer is the restriction of methionine, an essential amino acid in one-carbon metabolism. Methionine is the most variable metabolite found in human plasma [11], and has a myriad of functions as a result of its location in one-carbon metabolism [12]. Dietary MR is known to extend lifespan [13,14], and improve metabolic health[15–17]. One-carbon metabolism, through its essential role in redox and nucleotide metabolism, is the target of frontline cancer chemotherapies such as 5-fluorouracil, and radiation therapy [18–20]. Indeed some cancer cell lines are auxotrophic for methionine [21] and depleting or restricting methionine from the diet may have anti-cancer effects in mice [22–24]. Therefore, we reasoned that MR could have broad anti-cancer properties by targeting a focused area of metabolism that would interact with the response to other therapies that also affect one-carbon metabolism.

MR alters metabolism in mouse liver and plasma after a long-term intervention [11], but its impact on acute time scales is less explored. We switched the diet of C57BL/6J male mice from chow to a control (0.86% methionine w/w) or MR diet (0.12% methionine w/w), and obtained plasma metabolite profiles over time (Fig. 1a). The metabolic dynamics were studied with a singular value decomposition (Fig. 1b and Extended Data Fig. 1a) and showed coordinated changes related to methionine and sulfur metabolism (Fig. 1b–c) that were confirmed with hierarchical clustering (Extended Data Fig. 1b). MR reduced the levels of methionine-related metabolites within two days, which were sustained throughout the intervention (Fig. 1d, Extended Data Table 1, and Extended Data Fig.1b–f). Given these rapid and specific effects, we sought to evaluate MR in a series of pre-clinical settings related to one-carbon metabolism. We first considered two RAS-driven colorectal PDX models bearing a KRAS^{G12A} (CRC119) or NRAS^{Q61K} (CRC240) mutation (Extended Data Fig. 2a). Mice were subjected to the control or MR diet when the tumour was palpable (treatment) or two weeks prior to inoculation (prevention) (Fig. 1e). MR inhibited tumour growth in CRC119 (p=5.71e-12 at the end point, two-tailed Student’s t-test), and showed an

effect in CRC240 (p=0.054 at the end point, two-tailed Student's t-test) (Fig. 1f). Similar or higher amounts of food intake were observed (Extended Data Fig. 2b), implying the inhibitory effect was not due to caloric restriction. To gain insights into metabolism, we profiled metabolites in tumour, plasma and liver and found in each case MR altered methionine and sulfur-related metabolism (Extended Data Fig. 2c–e). A comparative metabolomics analysis across tissues concluded that these effects most likely occur in a cell autonomous manner (Methods, Extended Data Fig. 3) and could be confirmed with data in cell culture (Extended Data Fig. 4). Thus, the inhibition of tumour growth is at least partially if not largely attributed to lower circulating methionine levels leading to cell autonomous effects on tumour.

5-FU targets thymidylate synthase [18], and is a frontline chemotherapy for colorectal cancer with therapeutic strategies achieving modest (~60-65%) responses [25,26]. We therefore tested whether MR could synergize with 5-FU in CRC119 (Fig. 2a). We delivered a tolerable low dose of 5-FU that alone showed no effect on tumour growth (Fig. 2b). However, MR synergized with 5-FU treatment, leading to a marked inhibition on tumour growth and a broad effect on metabolic pathways in tumour, plasma and liver, with the most prominent changes to nucleotide metabolism and redox state related to both the mechanistic action of 5-FU and MR (Fig. 2b–d and Extended Data Fig. 5a–g). Fold changes of metabolites were highly correlated between plasma and liver (Spearman's rho = 0.38, p = 6.7e-11), but not between tumour and liver (Spearman's rho = 0.14, p = 0.02) or circulation (Spearman's rho = 0.14, p = 0.03) indicating that MR exerted specific effects on tumour (Extended Data Fig. 5h). Together, dietary MR synergizes with 5-FU, inhibiting CRC tumour growth and disrupting nucleotide metabolism and redox balance.

Next, nutrients related to methionine metabolism were supplemented to primary CRC119 cells and HCT116 colorectal cancer cells in the presence of MR or together with 5-FU (Extended Data Fig. 6a–b, Fig. 2e). Nucleosides, and N-acetylcysteine (NAC) along with related supplements partially alleviated the inhibition of cell proliferation due to MR or MR plus 5-FU in CRC119 cells (Fig. 2f). These observations were largely replicated in HCT116 cells (Extended Data Fig. 6b). Using U-^{13}C-Serine, we found MR led to reduction of M+1 dTTP, with an increase of M+1 methionine (Fig. 2g–h and Extended Data Fig. 6c). Thus, the synergistic effect between MR and 5FU is at least partially due to an increase in methionine synthesis, competing with dTMP synthesis for the serine-derived one-carbon unit, 5,10-methylene-tetrahydrofolate. Together, these data support the conclusion that nucleotide metabolism and redox balance contribute to MR-inhibited cell proliferation.

To further explore the therapeutic potential of dietary MR and related mechanisms, we considered an autochthonous model of radiation resistance in soft-tissue sarcoma [27]. Extremity sarcomas were induced in *FSF-Kras$^{G12D/+}$; p53$^{FRT/FRT}$* mice within 2-3 months after intramuscular delivery of adenovirus expressing FlpO recombinase (Methods, Fig. 3a). Autochthonous and PDX models together span the spectrum of acceptable pre-clinical tumour models and these cancer types allow for the investigation of treatments related to one-carbon metabolism (i.e. chemotherapy in CRC and radiation in sarcoma). MR alone did not alter tumour growth in this aggressive model, and led to minimal effects on methionine metabolism (Fig. 3b and Extended Data Fig. 7a–b). Strikingly, MR with a focal dose of 20

Gy reduced tumour growth and extended the tumour tripling time by 52%, from an average of 17.48 days to 26.57 days (Fig. 3c), comparable to effects seen with known radiosensitizing agents[28]. These effects appeared to be tumour cell autonomous and not attributable to protein synthesis or methylation reactions (Extended Data Fig. 7c–e). Nevertheless, disruptions to nucleotide and redox related metabolism were observed and may underlie the effects of MR plus radiation (Fig. 3d–e and Extended Data Fig. 7c–g).

Finally, in a proof-of-principle clinical study, 6 healthy middle-aged individuals were recruited and subjected to a low methionine (MR, ~2.92 mg/kg/day) diet, equivalent to 83% of reduction of daily methionine intake, for three weeks (Methods, Fig. 4a). MR reproducibly suppressed methionine levels, and altered circulating metabolism with cysteine and methionine metabolism among the top altered metabolic pathways (Fig. 4b and Extended Data Fig. 8a–c). MR reduced NAC and glutathione in all subjects, and affected metabolites related to methylation, nucleotide metabolism, tricarboxylic acid cycle, and amino acid metabolism (Fig. 4b–c and Extended Data Fig. 8d). Strikingly, plasma methionine-related metabolites in healthy humans were highly correlated with all animal models (Spearman's rho = 0.53 – 0.73) (Extended Data Fig. 9a–b, Fig. 4d), indicating a conserved response to MR. This controlled clinical study extends observations in methionine free diets that are toxic [29,30] to MR at levels that are tolerated in humans and provide reasonable dietary possibilities including what is possibly obtained in vegan or some Mediterranean diets.

Together, we provide evidence that dietary MR induces rapid, specific metabolic profiles in mice and humans that could be induced in a clinical setting. By disrupting the flux backbone of one-carbon metabolism with MR, vulnerabilities are created involving redox and nucleotide metabolism that can be exploited by administration of other therapies (in this case, radiation and antimetabolite chemotherapy) that target these aspects of cancer metabolism (Fig. 4e). Thus, a synthetic lethal interaction is defined with the diet and the otherwise resistant treatment modality. This study may further establish principles of how dietary interventions may be used to influence cancer outcomes in broader contexts.

METHODS

Animals, diets, and tissue harvesting

All animal procedures and studies were approved by the Institutional Animal Care and Use Committee (IACUC) at Duke University. All experiments were performed in accordance with relevant guidelines and regulations. All mice were housed at 20 ± 2°C with 50 ± 10% relative humidity and a standard12 h dark-12 h light cycle. The special diets with defined methionine levels used previously [11,16] were purchased from Research Diets (New Brunswick, NJ, USA) with the control diet contained 0.86% methionine (w/w, catalog #: A11051302) and MR diet contained 0.12% methionine (w/w, catalog #: A11051301). Three mouse models were employed and described below. For all animal studies, mice were randomized to the control or MR diet, and investigators were not blinded to allocation during experiments or outcome assessment.

Methionine restriction time course study in healthy mice

12-week-old male C57BL/6J mice (Jackson Laboratories, Bar Harbor, ME, USA) were subjected to either the control or the MR diet *ad libitum* for 3 weeks. Mouse blood was sampled through tail bleeding in the morning (10:00 am-12:00 am) at days 1, 2, 4, 7, 10, 14, 17, 21 post-dietary treatments. By day 21, all mice were sacrificed for tissue collection.

Colorectal cancer PDX models

PDXs of colorectal cancer with liver metastasis were developed as described previously [31,32] under an IRB approved protocol (Pro00002435). Briefly, CRC119 and CRC240 tumours were resected, washed and minced, and then passaged through JAX NOD.CB17-PrkdcSCID-J mice 2-5 times. For the dietary studies, CRC119 and CRC240 PDX tumours were minced in PBS at 150 mg/ml and 200 μl of tumour suspension were subcutaneously injected into the flanks of NOD.Cg-Prkdc^{scid} Il2rg^{tm1Wjl}/SzJ mice from the Jackson Laboratory. Mice (4 female + 3-4 male) were subjected to the control or MR diet either two weeks prior to the tumour injection or when the tumour was palpable until the end point (tumour volume ~1,500 mm$^{3)}$. Tumour size was monitored two to three times per week until the end point. For the combination therapy with a standard chemo drug 5-FU, mice were subjected to the control or the MR diet two weeks prior to the tumour injection until the end point. When tumours were palpable, mice (4 female + 4 male) were randomized to treatment of 5-FU (NDC 63323-117-10, 12.5 mg/kg three times per week) or vehicle (saline) through intraperitoneal injection. To minimize toxicity, we delivered an established low dose of 5-FU[33]. Tumour size was monitored two to three times per week until the end point.

Autochthonous soft tissue sarcomas

Primary soft-tissue sarcomas were generated as described previously [27,34]. Briefly, *p53^{FRT}* mice were crossed with mice carrying an Flp-activated allele of oncogenic Kras (*FSF-Kras^{G12D}*) to generate FSF-*Kras$^{G12D/+}$;p53$^{FRT/FRT}$* (*KP*) compound conditional mutant mice. *p53^{FRT}* mice and *FSF-Kras^{G12D}* mice were maintained on mixed C57BL/6J × 129SvJ backgrounds. Soft tissue sarcomas were induced by intramuscular injection of Ad-FlpO into *KP^{FRT}* mice. 25 μl Ad5CMVFlpO (6 × 10^{10} PFU/ml) was incubated with 600 μl minimum essential media (Sigma-Aldrich, St Louis, MO) and 3 μl 2 M $CaCl_2$ (Sigma-Aldrich, St Louis, MO) for 15 minutes to form calcium phosphate precipitates. 50 μl precipitated virus was injected intramuscularly per mouse to generate sarcomas. Soft tissue sarcomas developed at the site of injection in the lower extremity as early as 2 months post injection. *FSF-KrasG12D* mice were kindly provided by Tyler Jacks at MIT and we previously generated p53^{FRT} mice at Duke University [27,34].

KP mice (mixed gender) were subjected to control or MR diet when tumours were palpable (~150 mm^3) until the end point when the tumour tripled. Tumour size was monitored 2-3 times per week. For combination therapy with radiation, KP mice with palpable tumours were subjected to a single dose of 20 Gy focal radiation that is moderately effective in this model[35] using the X-RAD 225Cx small animal image-guided irradiator (Precision X-Ray). The irradiation field was centered on the target via fluoroscopy with 40 kilovolt peak (kVp), 2.5 mA x-rays using a 2-mm aluminum filter. Sarcomas were irradiated with parallel-opposed anterior and posterior fields with an average dose rate of 300 cGy/min prescribed to

midplane with 225 kVp, 13 mA x-rays using a 0.3-mm copper filter and a collimator with a 40 × 40 mm^2 radiation field at treatment isocenter. The dose rate was monitored in an ion chamber by members of the Radiation Safety Division at Duke University. After radiation, mice were subjected to the control or the MR diet immediately until the end point when tumour tripled. Tissues (tumour, liver and plasma) were collected at the time of tumour tripling. For metabolomics analysis, another cohort of mice on the combination therapy with radiation was sacrificed at 10 days post radiation and dietary treatment, the average time point when the KP mice on the control or MR diet alone had their tumour size tripled.

Tissue collection

For tissue collection from all the above animal studies, mice were fasted in the morning for 4 h (9:00-13:00). Tumour, plasma and liver were collected followed by immediate snap frozen, and stored at − 80°C until processed.

Colorectal cancer cell lines

Early passage primary CRC119 and CRC240 colorectal cancer cell lines were developed from the PDXs. PDXs were harvested and homogenized, and the homogenates were grown in RPMI 1640 media with addition of 10% fetal calf serum, 100,000 U/L penicillin and 100 mg/L streptomycin at 5% CO_2. A single cell clone was isolated using an O ring. The HCT116 cell line was a gift from Dr. Lewis Cantley's laboratory, and was maintained in RPMI 1640 supplemented with 10% fetal bovine serum and 100,000 U/L penicillin and 100 mg/L streptomycin. Cells were grown at 37 °C with 5% CO_2. Cell lines were authenticated at the Duke University DNA Analysis Facility by analyzing DNA samples from each cell lines for polymorphic short tandem repeat (STR) markers using the GenePrint 10 kit from Promega (Madison, WI, USA). All cell lines were negative for mycoplasma contamination.

Cell viability assay

Cell viability was determined by MTT assays. Briefly, cells cultured at 96-well plates were incubated in RPMI medium containing MTT (final concentration 0.5 mg/ml) at cell incubator for 2-4 hours. Media were then removed and replaced with 100 μl of DMSO, followed by additional 10 min of incubation at 37 °C. The absorbance at 540 nm was read using a plate reader. For the metabolite rescue studies, 10 μM of methionine that is one tenth of the amount in RPMI media is employed to approximately model dietary MR. We evaluated the effects of supplementation of a suite of nutrients related to methionine metabolism and the observed differences in metabolite profiles of CRC mouse models, including one-carbon donors, choline and formate; sulfur-donor homocysteine with or without cofactor Vitamin B12; nucleosides, and antioxidant N-acetylcysteine (NAC) on MR alone or in combination with 5-FU caused defects in cell proliferation. The following final conditions of metabolites were used: homocysteine (400 μM), B12 (20 μM), nucleosides (Millipore, 1×), choline (1 mM), formate (0.5 mM), NAC (1 mM), 5-FU (2.5 μM).

Human dietary study

The controlled feeding study was conducted at Penn State University Clinical Research Center (CRC) and approved by the Institutional Review Board of the Penn State College of

Medicine in accordance with the Helsinki Declaration of 1975 as revised in 1983 (IRB# 32378). We have complied with all relevant ethical regulations. Healthy adults of mixed gender were recruited by fliers and word of mouth and, as assessed for initial eligibility by telephone interview, were free of disease and currently not taking certain medications including anti-inflammatory drugs, corticosteroids, statins, thyroid drugs, and oral contraceptives. Final eligibility was assessed by standard clinical chemistry and hematology analyses. Written consent was obtained from eligible subjects and baseline resting metabolic rate was assessed by indirect calorimetry (Parvo Medics), physical activity by questionnaire and dietary intake by 3 unannounced 24 h diet recalls conducted by telephone in the week prior to returning to the clinic. All subjects, 6 healthy adults (5 females and 1 male) with a mean ± s.d. age of 52.2 ± 3.19 years (range: 49-58 years) and body mass index of 27.6 ± 4.32 kg/m^2, were placed on an MR diet for the final 3 weeks which provided 50-53% of energy from carbohydrate, 35-38% from fat, and 12-13% from protein and total calories adjusted individually based upon the baselines of resting metabolic rate and physical activity (calculated by the Harris Benedict Equation). Of the total protein, 75% was provided by a methionine-free medicinal beverage (Hominex-2, Abbott Nutrition, Columbus, OH) and the remaining 25% was from low methionine foods such as fruits, vegetables and refined grains. The total methionine intake was ~2.92 mg//kg/day, representing an 83% reduction in methionine intake compared to pre-test values from diet recalls (~17.2 mg/kg/d in the baseline level). The five-day cycle menu was created and evaluated for nutrient content using the Nutrition Data System for Research (2006, Minneapolis, MN). Blood was sampled into EDTA tubes in the morning after overnight fasting by a registered nurse at the beginning and end of the diet period. Plasma was obtained after centrifugation at 5,000 rpm for 10 min at 4°C. All 6 subjects agreed to have their samples and data used for future research. Biosamples were anonymized by re-coding. There was no registration or pre-registration of this study.

Metabolite profiling and isotope tracing

PDX primary cell lines were seeded in 6-well plates at a density of 2.0×10^5 cells per well. For overall polar metabolite profile, after overnight incubation, cells were washed once with PBS and cultured for an additional 24 h with 2 ml of conditional RPMI medium containing 0 μM or 100 μM methionine plus 10% FBS. Cellular metabolites were extracted after incubation. For U-^{13}C-Serine isotope tracing, both primary CRC119 cells and HCT116 cells were seeded in 6-well plates at a density of 2.0×10^5 cells per well. Cells were washed once with PBS after overnight incubation and cultured for an additional 24 h with 2 ml of conditional RPMI medium containing 0 μM or 100 μM methionine with or without addition of 5-FU (3.4 or 10 μM) plus 10% FBS. Then, medium was replaced with fresh conditional RPMI medium (0 μM or 100 μM methionine) with or without addition of 5-FU (3.4 or 10 μM) containing tracer U-^{13}C-Serine plus 10% dialyzed FBS. Cells were traced for 6 h, and followed by cellular metabolite extraction.

Metabolite extraction

Polar metabolite extraction has been described previously[36]. Briefly, tissue samples, liver and tumour, were pulverized in liquid nitrogen and then 3-10 mg of was weighed out for metabolite extraction using ice cold extraction solvent (80% methanol/water, 500 μl). Tissue

was then homogenized with a homogenizer to an even suspension, and incubated on ice for an additional 10 min. The extract was centrifuged at 20,000 g × 10 min at 4 °C. The supernatant was transferred to a new Eppendorf tube and dried in vacuum concentrator. For serum or medium, 20 μl of sample was added to 80 μl ice cold water in an Eppendorf tube on ice, followed by the addition of 400 μl ice cold methanol. Samples were vortexed at the highest speed for 1 min before centrifugation at 20,000 g for 10 min at 4 °C. For cells cultured in 6-well plates, cells were placed on top of dry ice right after medium removal. 1 ml ice-cold extraction solvent (80% methanol/water) was added to each well and the extraction plate was quenched at −80 °C for 10 min. Cells were then scraped off the plate into an Eppendorf tube. Samples were vortexed and centrifuged as described early. The supernatant was transferred to a new Eppendorf tube and dried in vacuum concentrator. The dry pellets were stored at −80 °C for LC-HRMS analysis. Samples were reconstituted into 30-60 μl sample solvent (water:methanol:acetonitrile, 2:1:1, v/v/v) and were centrifuged at 20,000 × *g* at 4 °C for 3 min. The supernatant was transferred to LC vials. The injection volume was 3 μl for HILIC chromatography, which is equivalent to a metabolite extract of 160 μg tissue injected on the column.

HPLC method

Ultimate 3000 UHPLC (Dionex) was coupled to Q Exactive-Mass spectrometer (QE-MS, Thermo Scientific) for metabolite separation and detection. For additional polar metabolite analysis, a hydrophilic interaction chromatography method (HILIC) with an Xbridge amide column (100 × 2.1 mm i.d., 3.5 μm; Waters) was used for compound separation at room temperature. The mobile phase and gradient information was described previously [37].

Mass spectrometry and data analysis

The QE-MS was equipped with a HESI probe, and the relevant parameters were as listed: heater temperature, 120 °C; sheath gas, 30; auxiliary gas, 10; sweep gas, 3; spray voltage, 3.6 kV for positive mode and 2.5 kV for negative mode. Capillary temperature was set at 320 °C, and S-lens was 55. A full scan range was set at 60 to 900 (m/z) when coupled with the HILIC method, or 300 to 1,000 (m/z) when low abundance metabolites need to be measured. The resolution was set at 70,000 (at m/z 200). The maximum injection time (max IT) was 200 ms. Automated gain control (AGC) was targeted at 3 Å~ 10^6 ions. LC-MS peak extraction and integration were analyzed with commercial available software Sieve 2.0 (Thermo Scientific). The integrated peak intensity was used for further data analysis. For tracing studies using U-^{13}C-Serine, ^{13}C natural abundance was corrected as previously described [38].

Statistical analysis and bioinformatics

Pathway analysis of metabolites was carried out with software Metaboanalyst (http://www.metaboanalyst.ca/MetaboAnalyst/) using the KEGG pathway database (http://www.genome.jp/kegg/). All data are represented as mean ± s.d. or mean ± s.e.m. as indicated. *P* values were calculated by a two-tailed Student's *t* test unless otherwise noted.

Analysis of the time-course metabolomics data

We first constructed a combinational matrix containing raw ion intensities of plasma metabolites from C57BL/6J mice, both the control and the MR groups. For each group there were 9 time points and 5 replicates for each time point, resulting in a 311 × 90 matrix. This matrix was then log-transformed and iteratively row-normalized and column-normalized until mean values of all rows and columns converged to zero. Singular value decomposition[39], was applied on the processed matrix to identify dominating dynamic modes:

$$A = U\Sigma V^T = \sum_{i=1}^{r} \sigma_i u_i v_i^T$$

In which A is the processed metabolomics matrix, σ_i is the ith singular value (ranked from maximal to minimal), $\sigma_i v_i^T$ is termed the ith mode. Modes 2 and 3 were defined as responding modes due to significant difference between control and MR values in both modes. For the ith metabolite, total contribution of modes 2 and 3 to its dynamics was evaluated by: $C_{23,i} = u_{i2}^2 + u_{i3}^2$. Mode 1 reflected an overall metabolic change due to switching diets at time zero. Modes 2 and 3 predominantly contained metabolites related to methionine and sulfur metabolism. Time-course metabolomics data of 50 metabolites with highest contribution of modes 2 and 3 was then clustered using clustergram() function in MATLAB R2018b. All methods used were implemented in MATLAB code. Hierarchical clustering confirmed that a set of methionine-related metabolites was most rapidly suppressed with other compensatory pathways changing at later times.

Cross-tissue comparison of metabolite fold changes (FC) in PDX and sarcoma models

Spearman's rank correlation coefficients were computed on metabolites measured in plasma, tumour and liver. Distance between FC in tissues A and B (*e.g.* liver and tumour) was computed by Euclidean distances between the two vectors of FC of all metabolites measured in both A and B.

Multidimensional scaling (MDS) was then applied to visualize the tissues in two-dimension, in which a stress function quantifying how accurate the pairwise distances between points are represented in the dimension-reduced coordinates compared to the original dataset was minimized:

$$\min \text{Stress}(x_1, \ldots, x_N) = \left(\frac{\sum_{ij} (d_{ij} - \|x_i - x_j\|)^2}{\sum_{ij} d_{ij}^2} \right)^{1/2}$$

$$x_1, \ldots, x_N \in \mathbb{R}^2$$

In which d_{ij} is the distance between the ith and jth data points in the original dataset and x_i means the ith point in the dimension-reduced dataset. All methods used here were implemented in MATLAB codes.

Methionine-related and -unrelated metabolites

To determine whether the effect of MR on tumour growth is systemic, cell autonomous, or both, we conducted an integrated analysis of global changes in the metabolic network across tumour, plasma and liver within each model from the prevention study in CRC PDX models in Fig. 1f. Methionine-related and -unrelated metabolites were defined according to their distance to methionine in the genome-scale metabolic model of human, Recon 2 [40]. Metabolites were defined as methionine-related if distance to methionine is less than or equal to 4, or methionine-unrelated when distance to methionine larger than 4. Metabolites were mapped by their KEGG IDs between the metabolomics dataset and Recon 2.

Quantitation of methionine concentrations

To quantify methionine concentrations in plasma, liver and tumour across the mouse models and in healthy humans, two additional datasets of metabolomics profiles in human plasma with their corresponding absolute methionine concentrations quantified using ^{13}C-labeled standards were used. The raw intensities across all samples were log-transformed and normalized. Linear regression was then performed on the normalized datasets to predict absolute methionine concentrations. Four normalization algorithms including cyclic loess, quantile, median and z-score were tested. Among the normalization algorithms, cyclic loess had the highest R-squared statistics in the corresponding linear regression model (R^2=0.74 for cyclic loess compared to 0.66 for quantile, 0.68 for median and 0.70 for z-score). Thus, the cyclic loess normalized dataset was used for the final model training, which generated the following equation describing the model:

$$\text{Log}\,[\mathit{Methionine}] = 1.001676\,\text{Log}I_{\mathit{Methionine}} - 14.446017$$

In this equation, [$\mathit{Methionine}$] is the absolute methionine concentration, and $I_{\mathit{Methionine}}$ is the cyclic loess normalized value of methionine intensity.

Data Availability

The metabolomics data reported in this study were deposited to Mendeley Data (DOI: doi: 10.17632/zs269d9fvb.1). All computer codes are available at: https://github.com/LocasaleLab/Dietary_methionine_restriction.

Extended Data

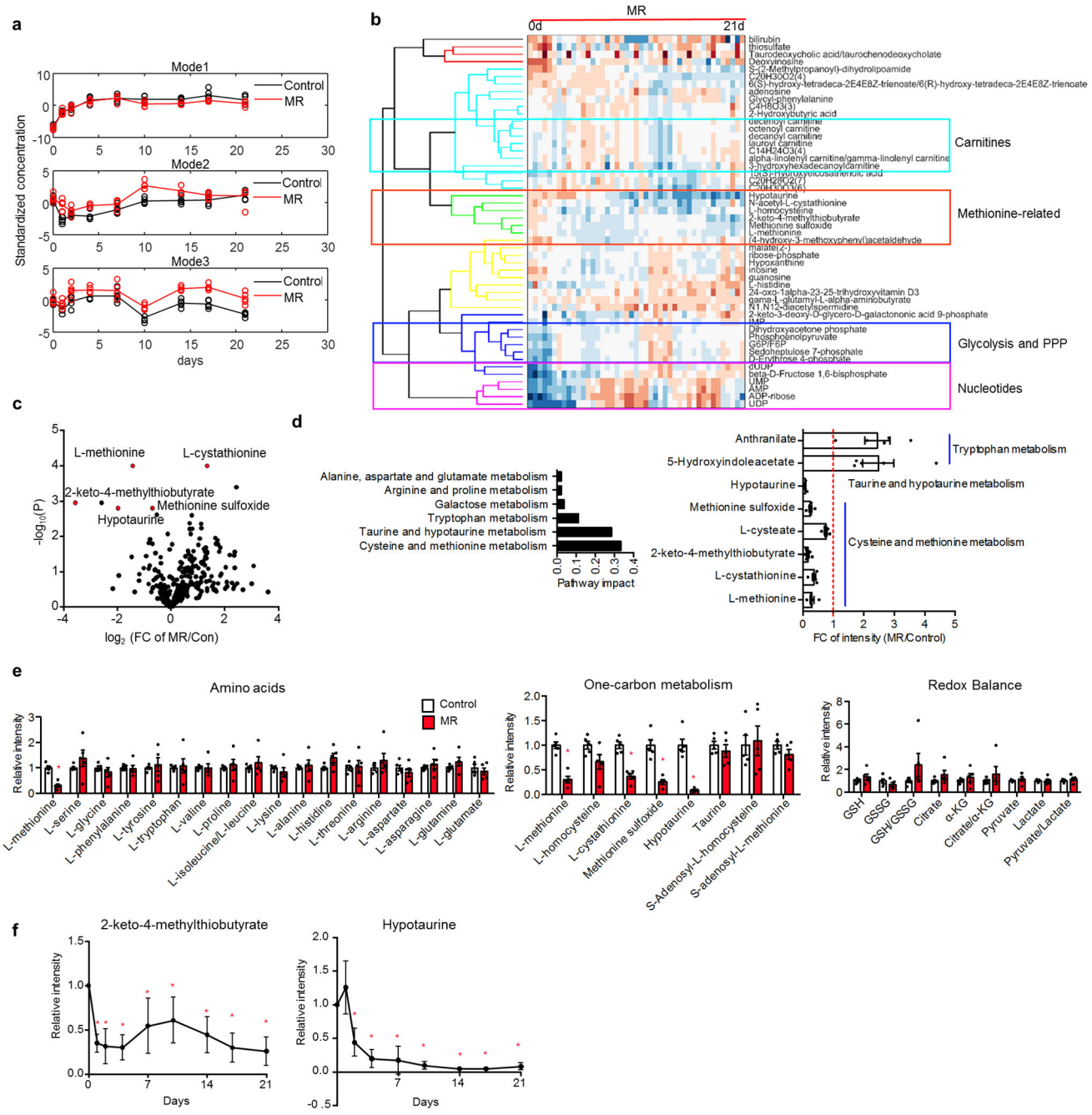

Extended Data Fig. 1. Dietary MR rapidly and specifically alters methionine and sulfur metabolism but maintains overall metabolism in healthy C57BL/6J mice

a, Dynamic patterns of top 3 modes. Standardized concentration (the values are normalized to have mean=0, standard deviation=1) in Mode 1, Mode 2 and Mode 3.

b, Heatmap of metabolites in Mode 2 and Mode 3.

c, Volcano plot of metabolites in plasma collected at the end point. FC, fold change. P values were determined by two-tailed Student's t-test.

d, Left: Pathway analysis of significantly changed (*p<0.05, two-tailed Student's t-test) plasma metabolites by 21-day MR diet. Right: FC of altered metabolites in the top three

most impacted pathways. Mean ± s.e.m., n=5 animals/group, *p<0.05, two-tailed Student's t-test.

e, Relative intensity of plasma amino acids and metabolites in one-carbon metabolism and redox balance at the end of study. Mean ± s.e.m., n=5 animals/group, *p<0.05, two-tailed Student's t-test.

f, Relative intensity of methionine metabolism related metabolite, 2-keto-4-methylthiobutyrate and hypotaurine. Mean ± s.d., n=5 animals/group, *p<0.05 by two-tailed Student's t-test.

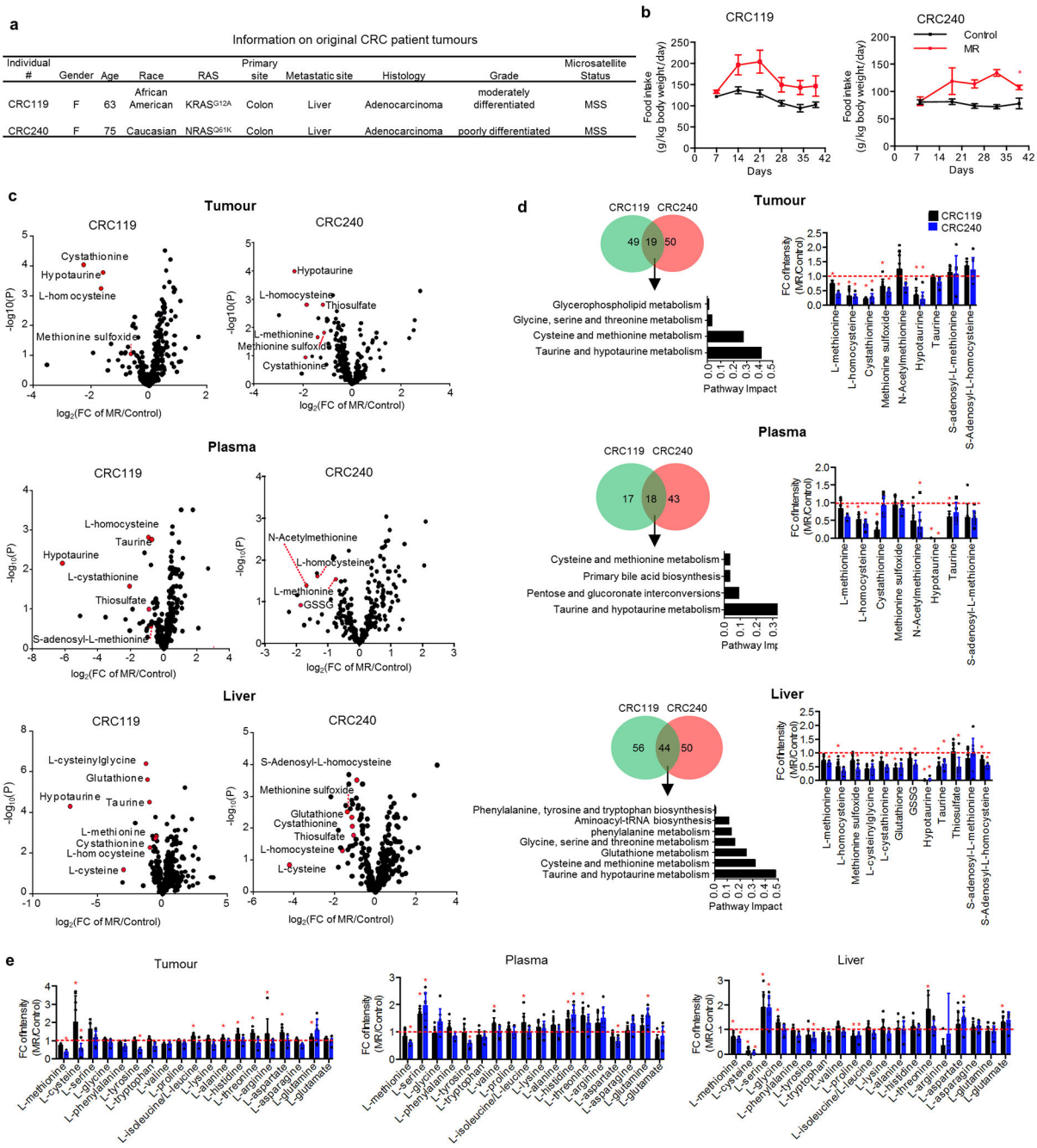

Extended Data Fig. 2. Dietary MR alters methionine metabolism in CRC PDX models

a, Information on original CRC patient tumours.

b-e, data from the prevention study in Fig. 1f. N=8 animals/group, 4 females + 4 males.

b, Food intake. Mean ± s.e.m., *p<0.05 by two-tailed Student's t-test.

c, Volcano plots of metabolites in tumours, plasma and liver. FC, fold changes. P values were determined by two-tailed Student's t-test.

d, Left: Venn diagram of significantly changed (*p<0.05, two-tailed Student's t-test) metabolites in tumour, plasma and liver by MR and pathway analysis (false discovery rate <

0.5) of the commonly changed metabolites; right: MR-induced FC of intensity of tumour metabolites in cysteine and methionine metabolism, and taurine and hypotaurine metabolism. Mean ± s.d., *p<0.05 by two-tailed Student's t-test. N=8 animals/group, 4 females + 4 males.

e, Relative FC of intensity of amino acids. Mean ± s.e.m., *p<0.05, two-tailed Student's t-test. N=8 animals/group, 4 females + 4 males.

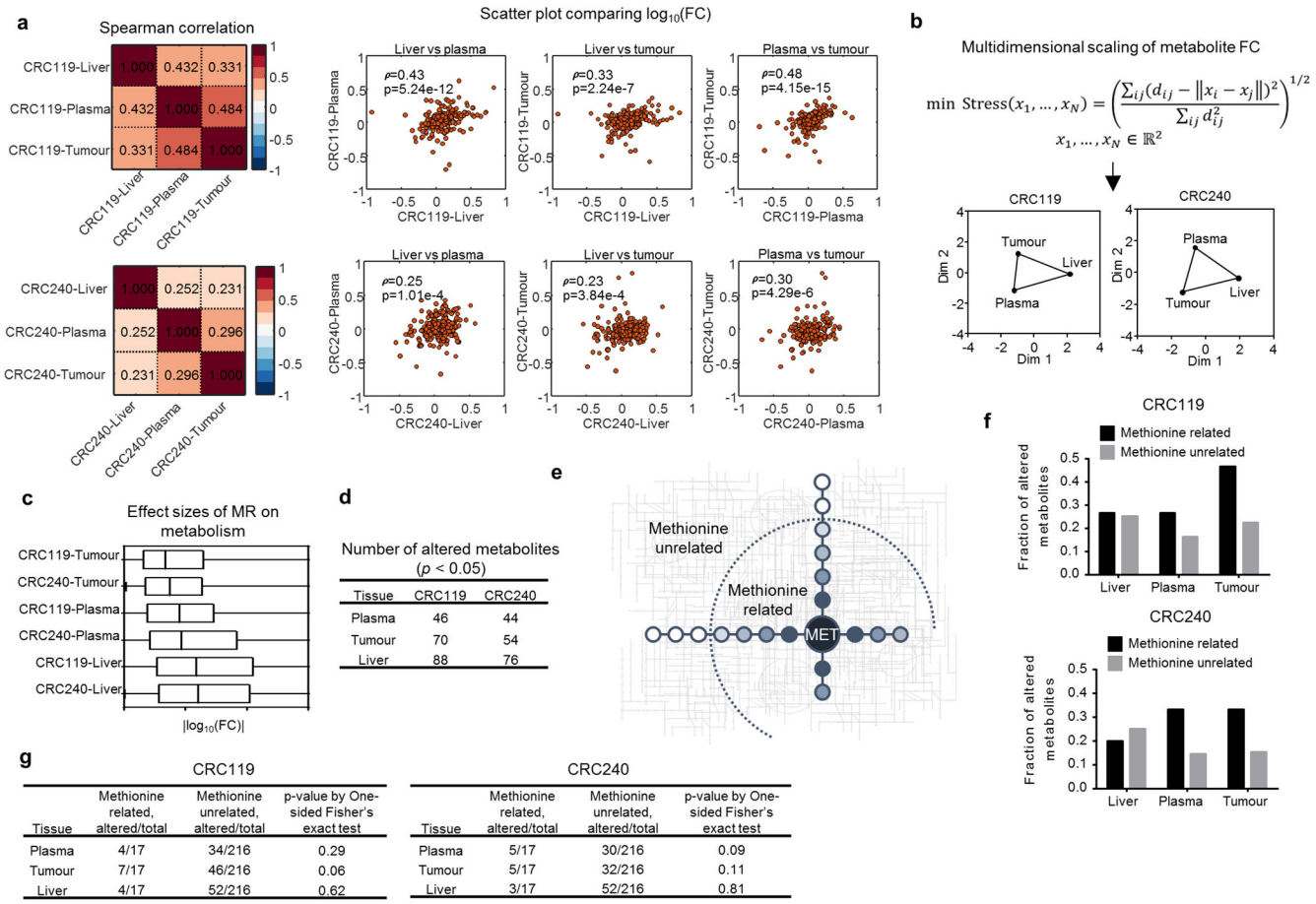

g

CRC119

Tissue	Methionine related, altered/total	Methionine unrelated, altered/total	p-value by One-sided Fisher's exact test
Plasma	4/17	34/216	0.29
Tumour	7/17	46/216	0.06
Liver	4/17	52/216	0.62

CRC240

Tissue	Methionine related, altered/total	Methionine unrelated, altered/total	p-value by One-sided Fisher's exact test
Plasma	5/17	30/216	0.09
Tumour	5/17	32/216	0.11
Liver	3/17	52/216	0.81

Extended Data Fig. 3. MR leads to specific cell intrinsic metabolic alterations in tumours

To determine whether the effect of MR on tumour growth is systemic, cell autonomous, or both, we conducted an integrated analysis of global changes in the metabolic network across tumour, plasma and liver within each model from the prevention study in Fig. 1f. N=8 animals/group, 4 females + 4 males.

a, Spearman's rank correlation coefficients of MR-induced FC of metabolites in tumour, plasma and liver exhibited strong correlations between each tissue pair with the highest correlation between tumour and plasma in both CRC119 and CRC240. FC, fold changes.

b, Multidimensional scaling analysis of metabolite FC in response to MR. In both models, the FC of metabolites in tumor showed a higher similarity with those in plasma than with those in liver.

c-d, Liver was the most affected tissue in both models. (c) Effect of MR on metabolism in tumour, plasma and liver evaluated by the $\log_{10}$ (FC). Box limits are the 25th and 75th percentiles, center lines are medians, and the whiskers are the minimal and maximal values. (d) Numbers of metabolites significantly altered (*p<0.05, two-tailed Student's t-test) by MR. N=8 animals/group, 4 females + 4 males.

e, Schematic defining methionine related (metabolized from or to methionine within 4 reaction steps) metabolites and otherwise methionine unrelated metabolites.

f-g, A higher proportion of altered metabolites was methionine-related in plasma and tumour compared to liver where MR-altered metabolites were nearly equally distributed between methionine-related and -unrelated groups. f, Fraction of significantly (*$p<0.05$, two-tailed Student's t-test) altered metabolites for methionine-related and methionine-unrelated metabolites in tumour, liver and plasma. g, Numbers of total and significantly altered metabolites for methionine-related and methionine-unrelated metabolites in tumour, liver and plasma and p value by one-sided Fisher's exact test.

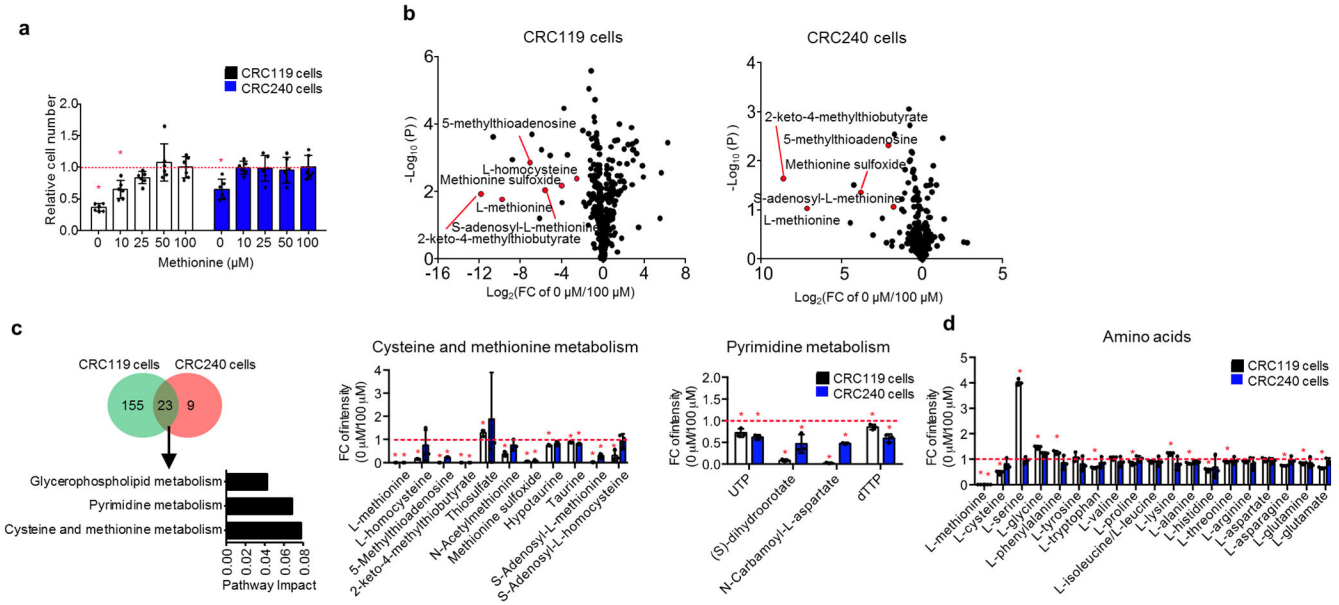

Extended Data Fig. 4. MR inhibits cell proliferation and most significantly alters cysteine and methionine in CRC primary cells

a, Relative cell numbers in CRC119 and CRC240 primary tumour cells treated with different doses of methionine for 72 h. Mean ± s.d., n = 3 biologically independent samples, similar results were obtained from three independent experiments, *p<0.05, two-tailed Student's t-test.

b, Volcano plots of metabolites in cells cultured in 0 or 100 μM methionine for 24 h. FC, fold changes. P values were determined by two-tailed Student's t-test.

c, Left: Venn diagram of significantly changed (*p<0.05, two-tailed Student's t-test) metabolites in CRC119 and CRC240 primary cells cultured with no methionine vs control (100 μM methionine), and pathway analysis of commonly changed metabolites. Right: FC of metabolites in the cysteine and methionine metabolism and pyrimidine metabolism in CRC119 and CRC240 primary cells treated with 0 or 100 μM methionine. Mean ± s.d., n = 3 biologically independent samples, *p<0.05, two-tailed Student's t-test.

d, Relative FC of intensity of amino acids by methionine deprivation in CRC119 and CRC240 primary cells. Mean ± s.d., n = 3 biologically independent samples, *p<0.05, two-tailed Student's t-test.

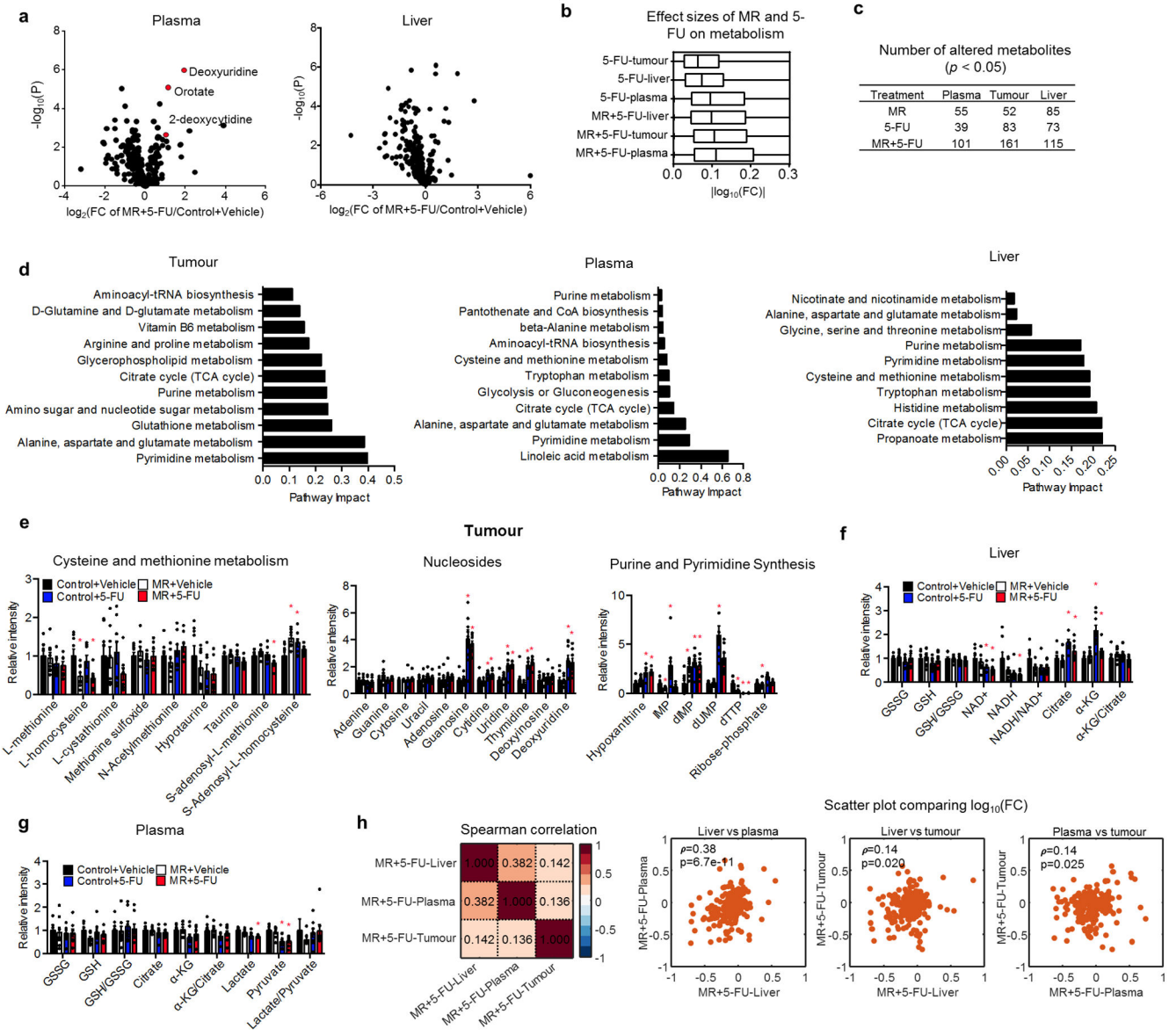

Extended Data Fig. 5. Dietary MR sensitizes CRC PDX models to chemotherapy 5-Fluorouracil (5-FU)

a, Volcano plots of metabolites in plasma and liver altered by the combination of dietary MR and 5-FU. FC, fold change. P values were determined by two-tailed Student's t-test.

b, Effect of 5-FU alone and a combination of MR and 5-FU on metabolites in tumour, plasma and liver evaluated by the $\log_{10}$ (FC). Box limits are the 25th and 75th percentiles, center lines are medians, and the whiskers are the minimal and maximal values. The data represents metabolites in liver (337), plasma (282), and tumour (332) from n= 8 animals/ group.

c, Numbers of metabolites significantly changed by MR, 5-FU or a combination of MR and 5-FU in plasma, tumour and liver. *p<0.05, two-tailed Student's t-test.

d, Pathway analysis of metabolites significantly changed (*p<0.05, two-tailed Student's t-test) by MR, 5-FU, or by the combination of dietary MR and 5-FU with false discovery rate < 0.5.

e-g, Relative intensity of metabolites related to cysteine and methionine metabolism and nucleotide metabolism in tumour (e) and redox balance in liver (f) and plasma (g). GSH, glutathione; GSSG, the oxidized form of glutathione; α–KG, α–ketoglutarate. Mean ± s.e.m., n = 8 animals/group, *p<0.05, two-tailed Student's t-test.

h, Spearman's rank correlation coefficients of MR and 5-FU-induced FC of metabolites in tumour, plasma and liver from mice on dietary MR and 5-FU.

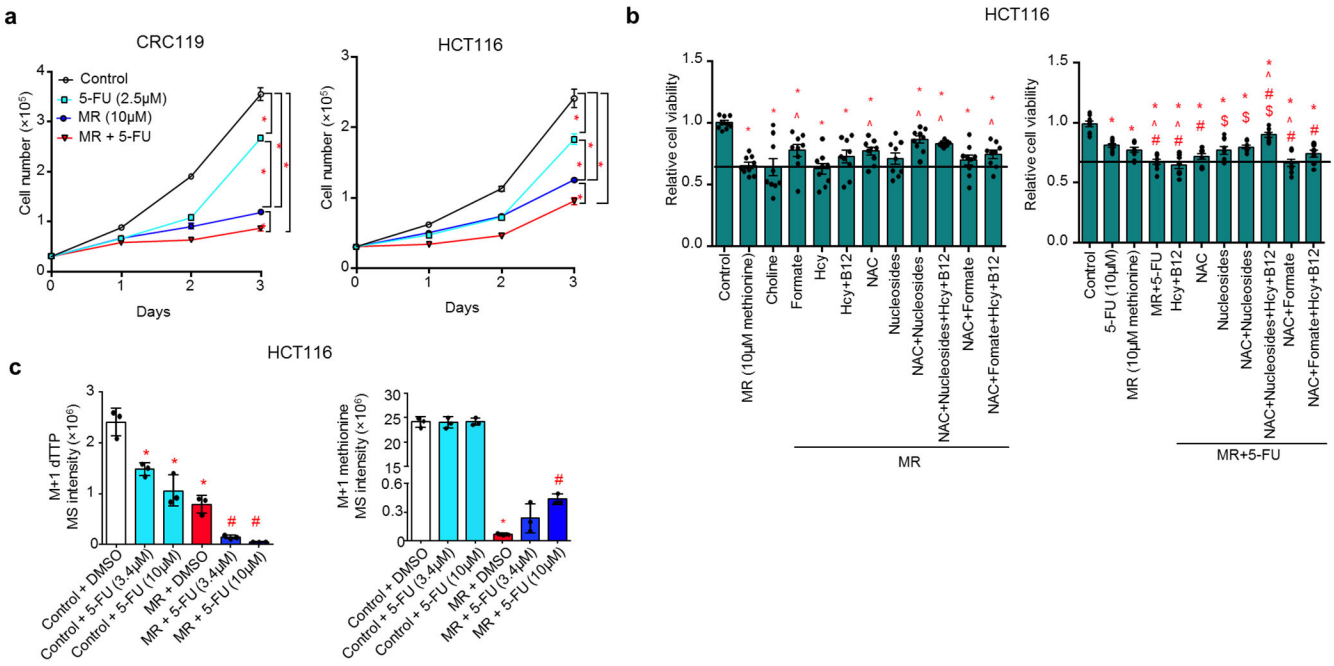

Extended Data Fig. 6. MR-mediated inhibition of cell growth is largely due to interruptions to nucleosides production and redox balance

a, Synergic effect of MR and 5-FU in CRC119 primary cells and HCT116 cells were evaluated by cell counting. Mean ± s.e.m., n=3 biological replicates, * $p<0.05$ by two-tailed Student's t-test.

b, Rescue effect of choline, formate, sulfur-donor homocysteine (Hcy), Hcy+B12, nucleosides, and antioxidant N-acetylcysteine (NAC) alone or in combination on MR-mediated inhibition of HCT116 cell proliferation. Mean ± s.e.m., n=9 biologically independent samples from three independent experiments, * $p<0.05$ vs control, ^ $p<0.05$ vs MR, # $p<0.05$ vs 5-FU; $ $p<0.05$ vs MR+5-FU by two-tailed Student's t-test.

c, Mass intensity for M+1 dTTP and M+1 methionine in HCT116 cells from experiment described in Fig. 2h. Mean ± s.d., n=3 biologically independent samples, *$p<0.05$ vs control and #$p<0.05$ vs MR by two-tailed Student's t-test.

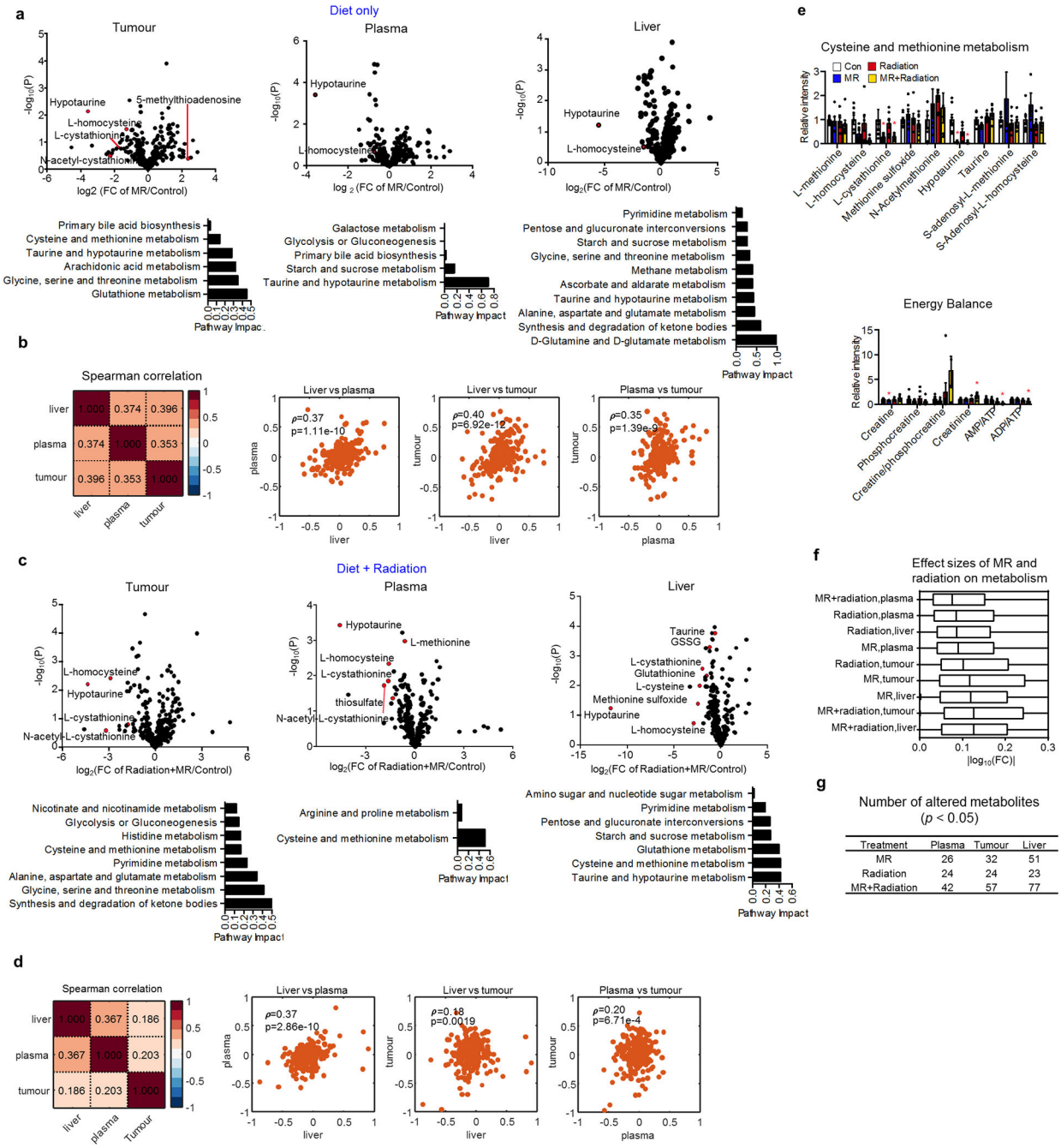

Extended Data Fig. 7. Dietary MR sensitizes RAS-driven autochthonous sarcoma mouse models to radiation

a, Volcano plots of metabolites in tumour, plasma and liver, and pathway analysis of metabolites significantly changed (*p<0.05, two-tailed Student's t-test) by dietary MR alone (false discovery rate < 1). FC, fold change.

b, Spearman's rank correlation coefficients of MR-induced FC of metabolites in tumour, plasma and liver.

c, Volcano plots of metabolites in tumour, plasma and liver, and pathway analysis of metabolites significantly changed (*p<0.05, two-tailed Student's t-test) by dietary MR and radiation (false discovery rate < 0.5).

d, Spearman's rank correlation coefficients of MR and radiation-induced FC of metabolites in tumour, plasma and liver.

e, Relative intensity of metabolites related to cysteine and methionine metabolism and energy balance in tumours. Mean ± s.d., n= 7 animals/group except for MR group (n=6), *p<0.05 vs control by two-tailed Student's t-test.

f-g, The largest effects on metabolism occurred in the combination of diet and radiation. f, Effect of MR and radiation alone or in combination on metabolites in tumour, plasma and liver evaluated by the $\log_{10}$ (FC). Box limits are the 25th and 75th percentiles, center lines are medians, and the whiskers are the minimal and maximal values. The data represents metabolites in liver (319), plasma (308), and tumour (332) from n= 7 animals/group except for MR group (n=6).

g, Numbers of metabolites significantly changed (*p<0.05, two-tailed Student's t-test) by MR and radiation alone or in combination.

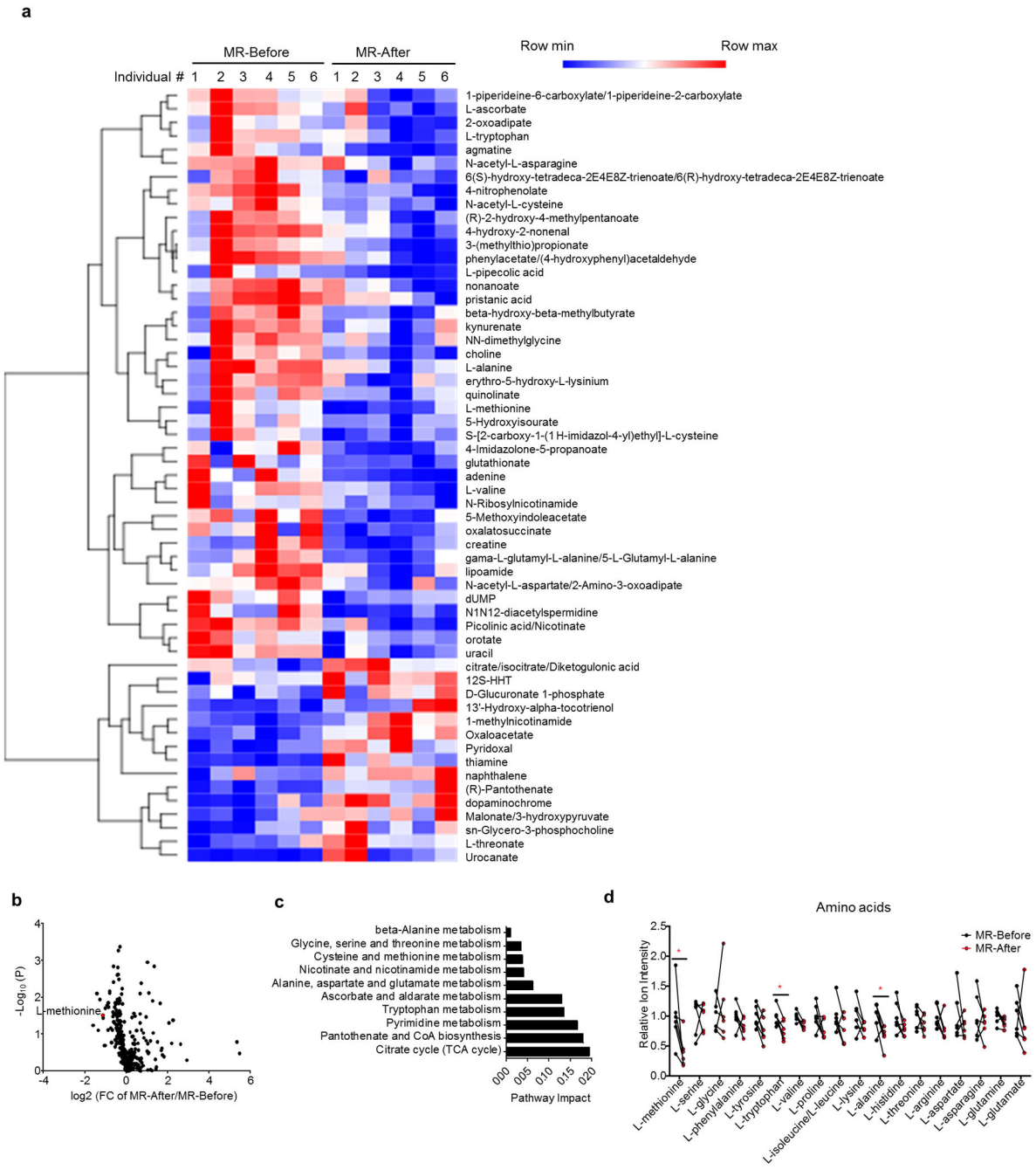

Extended Data Fig. 8. Dietary MR can be achieved in humans

a, Heatmap of significantly changed (*p<0.05, two-tailed Student's t-test) plasma metabolites by dietary intervention in six human subjects.

b, Volcano plot of plasma metabolites. FC, fold change. P values were determined by two-tailed Student's t-test.

c, Pathway analysis of altered (*p<0.05, two-tailed Student's t-test) plasma metabolites.

d, Relative intensity of amino acids in plasma. N= biologically independent humans, *p<0.05 by two-tailed Student's t-test.

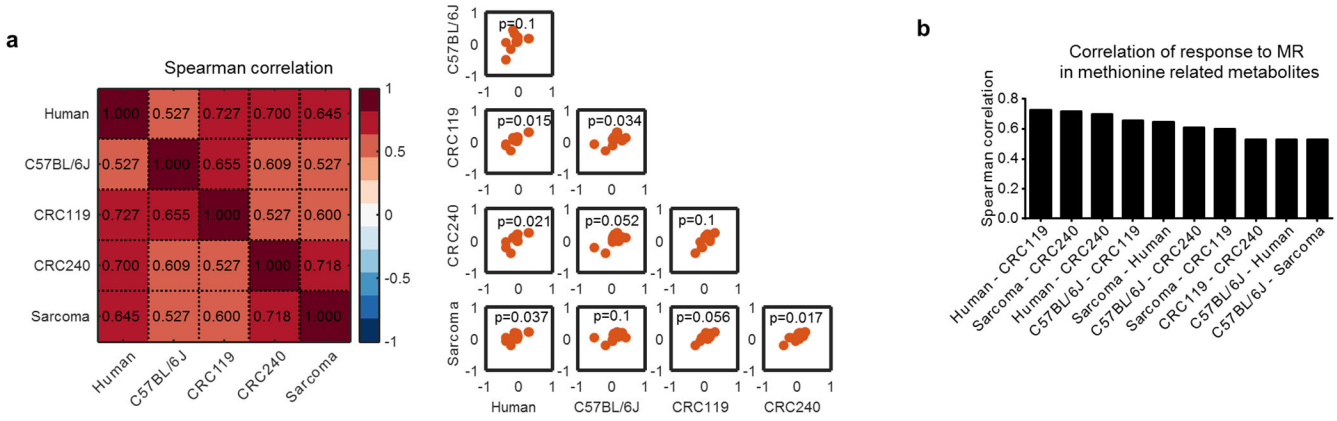

Extended Data Fig. 9. Comparative metabolic effects of MR across mouse models and humans

a, Spearman's rank correlation coefficients of MR-induced fold changes of methionine-related metabolites (defined in Extended Data Fig. 3f) in plasma samples from non-tumour bearing C57BL/6J mice, PDX CRC119 and CRC240 mouse models, sarcoma mouse model, and healthy human subjects.

b, Spearman's rank correlation coefficients among different models in a ranked from the highest to the lowest.

Extended Data Table 1.
Methionine concentrations in plasma, tumour and liver across mouse models and humans

Tissues were collected at the end of each experiment. Concentrations in tissues were estimated in μM, assuming 1 g wet tissue weight = 1 ml. Quantitation was performed by using ^{13}C-labeled standards for each amino acid, which were added before extraction. Cyclic Loess normalization and linear regression was applied in quantitation of methionine in samples without ^{13}C-labeled standards.

Model	Tissue	Control diet	MR diet
CRC119	Plasma	37.58 ± 6.08	27.44 ± 4.28 *
	Tumour	31.23 ± 9.10	20.08 ± 2.36 *
	Liver	29.99 ± 2.38	18.68 ± 4.12 *
CRC240	Plasma	52.35 ± 12.19	32.98 ± 3.60 *
	Tumour	70.77 ± 25.73	31.82 ± 3.05 *
	Liver	18.97 ± 3.10	12.393 ± 1.86 *
CRC119 (Vehicle)	Plasma	35.93 ± 6.02	33.88 ± 7.97
	Tumour	33.52 ± 10.31	31.50 ± 12.12
	Liver	17.37 ± 4.18	16.68 ± 3.88
CRC119 (5-FU)	Plasma	32.13 ± 5.29	31.31 ± 11.55
	Tumour	26.70 ± 7.15	29.45 ± 11.04
	Liver	16.50 ± 5.14	16.61 ± 2.39

Model	Tissue	Control diet	MR diet
Sarcoma	Plasma	37.75 ± 5.27	35.86 ± 14.57
	Tumour	46.84 ± 10.01	38.39 ± 10.32
	Liver	10.44 ± 4.74	10.45 ± 3.44
Sarcoma (Radiation)	Plasma	24.44 ± 7.56	25.87 ± 4.11 #
	Tumour	43.10 ± 11.86	37.22 ± 4.97 #
	Liver	10.43 ± 2.98	6.55 ± 1.9 *
C57BL/6J	Plasma	99.89 ± 16.90	28.79 ± 4.59 *
Human	Plasma	13.74 ± 5.19	6.55 ± 4.02 *

Values are mean ± s.d.; n= 8 for CRC119, CRC240, CRC119 (Vehicle) and CRC119 (5-FU), 7 for sarcoma on the control diet, 6 for sarcoma on the MR diet, 7 for sarcoma (Radiation), 5 for C57BL/6J, 6 for humans;

* $p < 0.05$ by two tailed Student's t-test between the control diet and the MR diet,

# $p < 0.05$ by two tailed Student's t-test between the control diet vs the MR diet + radiation.

ACKNOWLEDGEMENTS

Support from the National Institutes of Health R01CA193256, R21CA201963, P30CA014236 (J.W.L.), R35CA197616 (D.G.K.), T32CA93240 (D.E.C.), and the Canadian Institutes of Health Research (CIHR, 146818) (X.G) are gratefully acknowledged. We thank Drs. Mary Lou Kiel and Terryl Hartman for their assistance in designing the diets and Sami Heim for her help with food preparation in the human study. The human study was partially supported by the CRC at Penn State University (NIH M01RR10732). We gratefully acknowledge members of the Locasale lab for helpful discussions and apologize to those whose work we couldn't cite due to space constraints.

REFERENCES

1. DeBerardinis RJ & Chandel NS Fundamentals of cancer metabolism. Sci Adv 2, e1600200, doi: 10.1126/sciadv.1600200 (2016). [PubMed: 27386546]
2. Goncalves MD, Hopkins BD & Cantley LC Dietary Fat and Sugar in Promoting Cancer Development and Progression. Annual Review of Cancer Biology 3, 255–273, doi:10.1146/annurev-cancerbio-030518-055855 (2019).
3. Cantor JR et al. Physiologic Medium Rewires Cellular Metabolism and Reveals Uric Acid as an Endogenous Inhibitor of UMP Synthase. Cell 169, 258–272 e217, doi:10.1016/j.cell.2017.03.023 (2017). [PubMed: 28388410]
4. Tardito S et al. Glutamine synthetase activity fuels nucleotide biosynthesis and supports growth of glutamine-restricted glioblastoma. Nat Cell Biol 17, 1556–1568, doi:10.1038/ncb3272 (2015). [PubMed: 26595383]
5. Liu X, Romero IL, Litchfield LM, Lengyel E & Locasale JW Metformin Targets Central Carbon Metabolism and Reveals Mitochondrial Requirements in Human Cancers. Cell Metab 24, 728–739, doi:10.1016/j.cmet.2016.09.005 (2016). [PubMed: 27746051]
6. Maddocks OD et al. Serine starvation induces stress and p53-dependent metabolic remodelling in cancer cells. Nature 493, 542–546, doi:10.1038/nature11743 (2013). [PubMed: 23242140]
7. Maddocks ODK et al. Modulating the therapeutic response of tumours to dietary serine and glycine starvation. Nature 544, 372–376, doi:10.1038/nature22056 (2017). [PubMed: 28425994]
8. Gravel SP et al. Serine deprivation enhances antineoplastic activity of biguanides. Cancer Res 74, 7521–7533, doi:10.1158/0008-5472.CAN-14-2643-T (2014). [PubMed: 25377470]
9. Kanarek N et al. Histidine catabolism is a major determinant of methotrexate sensitivity. Nature, doi:10.1038/s41586-018-0316-7 (2018).

10. Knott SRV et al. Asparagine bioavailability governs metastasis in a model of breast cancer. Nature 554, 378–381, doi:10.1038/nature25465 (2018). [PubMed: 29414946]
11. Mentch SJ et al. Histone Methylation Dynamics and Gene Regulation Occur through the Sensing of One-Carbon Metabolism. Cell Metab 22, 861–873, doi:10.1016/j.cmet.2015.08.024 (2015). [PubMed: 26411344]
12. Gao X, Reid MA, Kong M & Locasale JW Metabolic interactions with cancer epigenetics. Mol Aspects Med 54, 50–57, doi:10.1016/j.mam.2016.09.001 (2017). [PubMed: 27620316]
13. Orentreich N, Matias JR, DeFelice A & Zimmerman JA Low methionine ingestion by rats extends life span. J Nutr 123, 269–274 (1993). [PubMed: 8429371]
14. Lee BC et al. Methionine restriction extends lifespan of Drosophila melanogaster under conditions of low amino-acid status. Nat Commun 5, 3592, doi:10.1038/ncomms4592 (2014). [PubMed: 24710037]
15. Malloy VL et al. Methionine restriction prevents the progression of hepatic steatosis in leptin-deficient obese mice. Metabolism 62, 1651–1661, doi:10.1016/j.metabol.2013.06.012 (2013). [PubMed: 23928105]
16. Ables GP, Perrone CE, Orentreich D & Orentreich N Methionine-restricted C57BL/6J mice are resistant to diet-induced obesity and insulin resistance but have low bone density. PLoS One 7, e51357, doi:10.1371/journal.pone.0051357 (2012). [PubMed: 23236485]
17. Malloy VL et al. Methionine restriction decreases visceral fat mass and preserves insulin action in aging male Fischer 344 rats independent of energy restriction. Aging Cell 5, 305–314, doi: 10.1111/j.1474-9726.2006.00220.x (2006). [PubMed: 16800846]
18. Ser Z et al. Targeting One Carbon Metabolism with an Antimetabolite Disrupts Pyrimidine Homeostasis and Induces Nucleotide Overflow. Cell Rep 15, 2367–2376, doi:10.1016/j.celrep. 2016.05.035 (2016). [PubMed: 27264180]
19. Miousse IR et al. One-carbon metabolism and ionizing radiation: a multifaceted interaction. Biomol Concepts 8, 83–92, doi:10.1515/bmc-2017-0003 (2017). [PubMed: 28574375]
20. Locasale JW Serine, glycine and one-carbon units: cancer metabolism in full circle. Nat Rev Cancer 13, 572–583, doi:10.1038/nrc3557 (2013). [PubMed: 23822983]
21. Hoffman RM & Erbe RW High in vivo rates of methionine biosynthesis in transformed human and malignant rat cells auxotrophic for methionine. Proc Natl Acad Sci U S A 73, 1523–1527 (1976). [PubMed: 179090]
22. Komninou D, Leutzinger Y, Reddy BS & Richie JP Jr. Methionine restriction inhibits colon carcinogenesis. Nutr Cancer 54, 202–208, doi:10.1207/s15327914nc5402_6 (2006). [PubMed: 16898864]
23. Hens JR et al. Methionine-restricted diet inhibits growth of MCF10AT1-derived mammary tumours by increasing cell cycle inhibitors in athymic nude mice. BMC Cancer 16, 349, doi:10.1186/ s12885-016-2367-1 (2016). [PubMed: 27255182]
24. Guo H et al. Therapeutic tumour-specific cell cycle block induced by methionine starvation in vivo. Cancer Res 53, 5676–5679 (1993). [PubMed: 8242623]
25. Saltz LB et al. Bevacizumab in combination with oxaliplatin-based chemotherapy as first-line therapy in metastatic colorectal cancer: a randomized phase III study. J Clin Oncol 26, 2013–2019, doi:10.1200/JCO.2007.14.9930 (2008). [PubMed: 18421054]
26. Douillard JY et al. Randomized, phase III trial of panitumumab with infusional fluorouracil, leucovorin, and oxaliplatin (FOLFOX4) versus FOLFOX4 alone as first-line treatment in patients with previously untreated metastatic colorectal cancer: the PRIME study. J Clin Oncol 28, 4697–4705, doi: 10.1200/JCO.2009.27.4860 (2010). [PubMed: 20921465]
27. Kirsch DG et al. A spatially and temporally restricted mouse model of soft tissue sarcoma. Nat Med 13, 992–997, doi: 10.1038/nm1602 (2007). [PubMed: 17676052]
28. Moding EJ et al. Tumour cells, but not endothelial cells, mediate eradication of primary sarcomas by stereotactic body radiation therapy. Sci Transl Med 7, 278ra234, doi: 10.1126/ scitranslmed.aaa4214 (2015).
29. Durando X et al. Optimal methionine-free diet duration for nitrourea treatment: a Phase I clinical trial. Nutr Cancer 60, 23–30, doi:10.1080/01635580701525877 (2008). [PubMed: 18444132]

30. Durando X et al. Dietary methionine restriction with FOLFOX regimen as first line therapy of metastatic colorectal cancer: a feasibility study. Oncology 78, 205–209, doi:10.1159/000313700 (2010). [PubMed: 20424491]
31. Kim MK et al. Characterization of an oxaliplatin sensitivity predictor in a preclinical murine model of colorectal cancer. Mol Cancer Ther 11, 1500–1509, doi:10.1158/1535-7163.MCT-11-0937 (2012). [PubMed: 22351745]
32. Uronis JM et al. Histological and molecular evaluation of patient-derived colorectal cancer explants. PLoS One 7, e38422, doi:10.1371/journal.pone.0038422 (2012). [PubMed: 22675560]
33. Udofot O et al. Pharmacokinetic, biodistribution and therapeutic efficacy of 5-fluorouracil-loaded pH-sensitive PEGylated liposomal nanoparticles in HCT-116 tumour bearing mouse. J Nat Sci 2 (2016).
34. Lee CL et al. Generation of primary tumours with Flp recombinase in FRT-flanked p53 mice. Dis Model Mech 5, 397–402, doi:10.1242/dmm.009084 (2012). [PubMed: 22228755]
35. Moding EJ et al. Atm deletion with dual recombinase technology preferentially radiosensitizes tumour endothelium. J Clin Invest 124, 3325–3338, doi:10.1172/JCI73932 (2014). [PubMed: 25036710]
36. Liu X et al. High resolution metabolomics with acyl-CoA profiling reveals widespread remodeling in response to diet. Mol Cell Proteomics, doi:10.1074/mcp.M114.044859 (2015).
37. Liu X, Ser Z & Locasale JW Development and quantitative evaluation of a high-resolution metabolomics technology. Anal Chem 86, 2175–2184, doi:10.1021/ac403845u (2014). [PubMed: 24410464]
38. Yuan J, Bennett BD & Rabinowitz JD Kinetic flux profiling for quantitation of cellular metabolic fluxes. Nat Protoc 3, 1328–1340, doi:10.1038/nprot.2008.131 (2008). [PubMed: 18714301]
39. Holter NS et al. Fundamental patterns underlying gene expression profiles: simplicity from complexity. Proc Natl Acad Sci U S A 97, 8409–8414, doi:10.1073/pnas.150242097 (2000). [PubMed: 10890920]
40. Thiele I et al. A community-driven global reconstruction of human metabolism. Nat Biotechnol 31, 419–425, doi:10.1038/nbt.2488 (2013). [PubMed: 23455439]

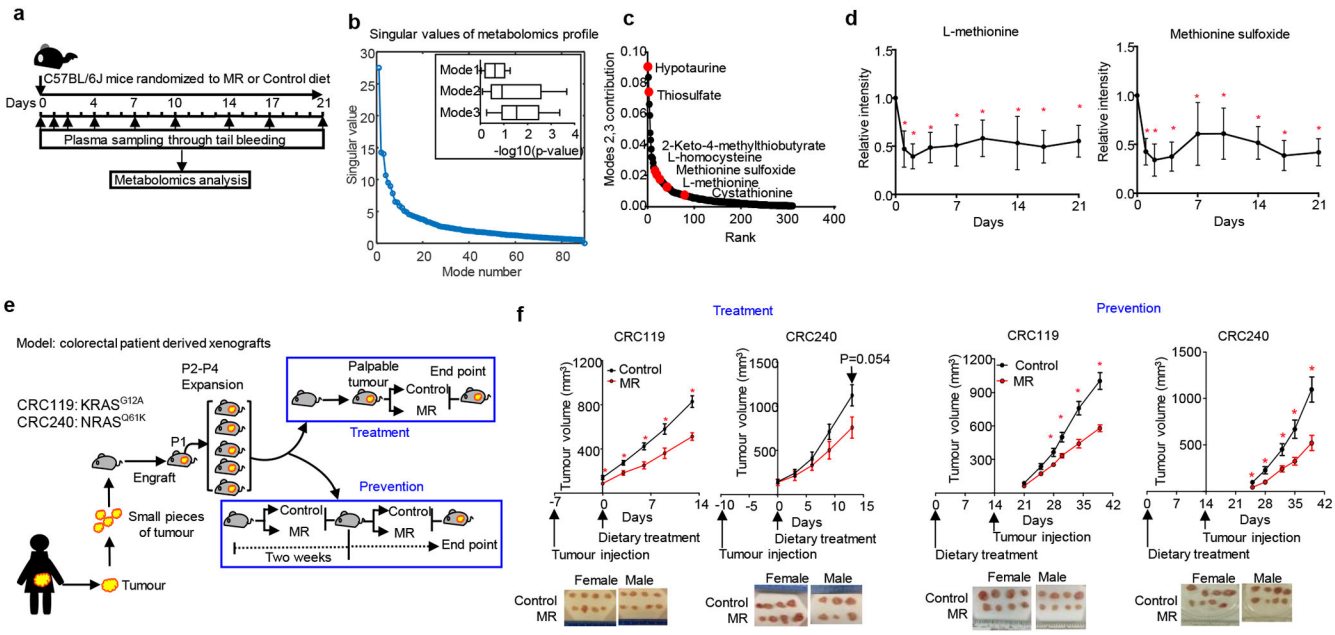

Fig. 1. Dietary MR rapidly and specifically alters methionine and sulfur metabolism and inhibits tumour growth in colorectal patient-derived xenograft (PDX) models

a, Experimental design in C57BL/6J mice. n=5 animals/group.

b, 90 sets of metabolic profiles from a were computed for singular values via singular value decomposition. Insertion: two-sided t-test p-values assessing difference between control and MR in the first three modes. n=5 animals/group. Box limits are the 25th and 75th percentiles, center lines are medians, and the whiskers are the minimal and maximal values.

c, Contribution of modes 2 and 3 in b ranked across all measured metabolites.

d, Relative intensity of methionine and methionine sulfoxide. Mean ± s.d., n=5 animals/group, *p<0.05 by two-tailed Student's t-test.

e, Schematic of experimental design using colorectal PDXs. Treatment: n=7/group, 4 females + 3 males, prevention: n=8/group, 4 females + 4 males.

f, Tumour growth curve and images of tumours at the end point from e. Mean ± s.e.m., *p<0.05 by two-tailed Student's t-test.

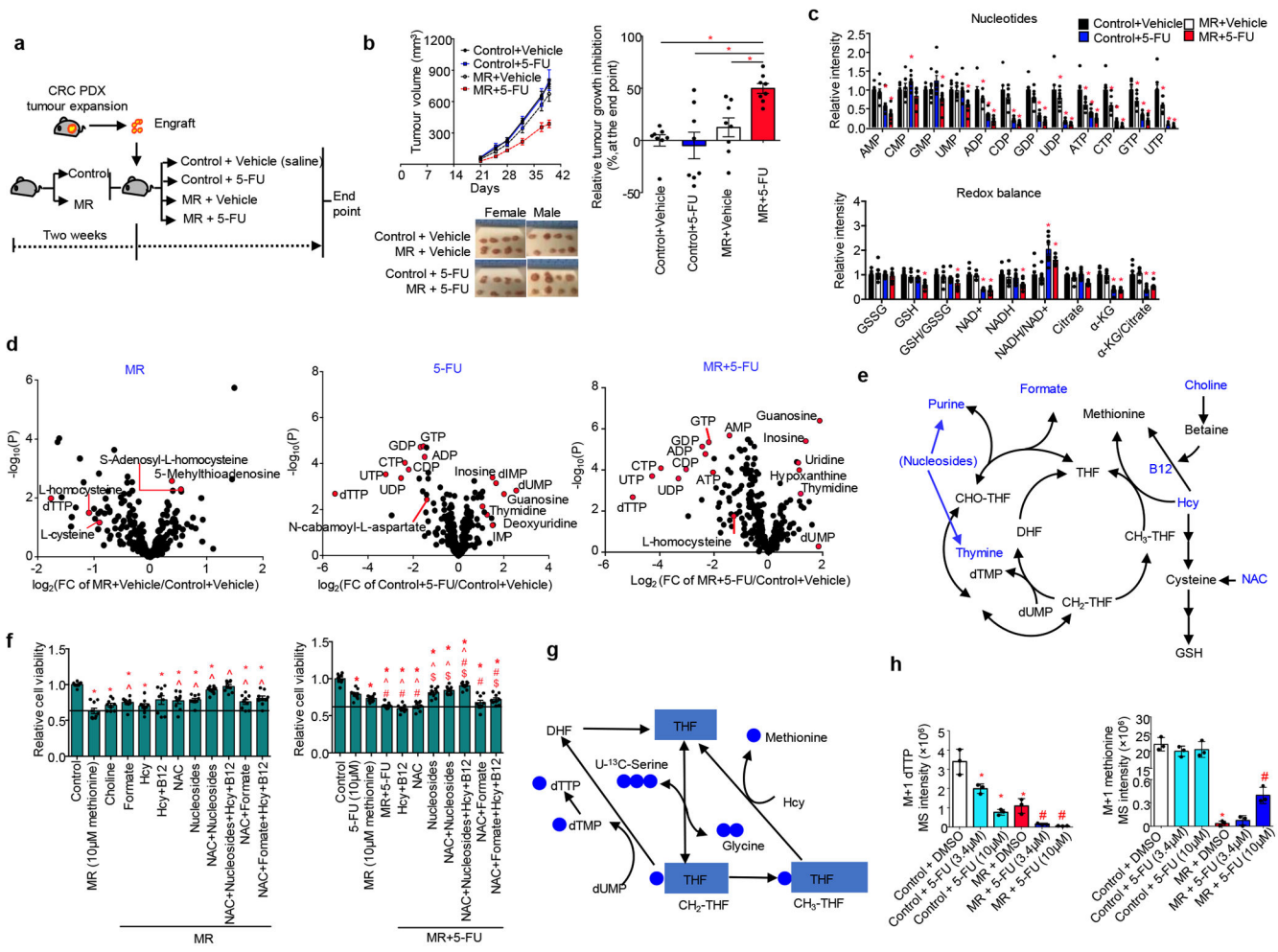

Fig. 2. Dietary MR sensitizes CRC PDX models to chemotherapy 5-Fluorouracil (5-FU)

a, Experimental design.

b, Tumour growth curves, quantitation, and images at the end point. Mean ± s.e.m., *p<0.05 by two-tailed Student's t-test. n=8 animals/group, 4 females + 4 males.

c, Relative intensity of metabolites related to nucleotide metabolism and redox balance in tumours. Mean ± s.e.m., *p<0.05 vs control by two-tailed Student's t-test. n=8 animals/group.

d, Volcano plots of metabolites in tumours. FC, fold change. P values were determined by two-tailed Student's t-test.

e, Schematic of supplementation experiments with added metabolites in blue. Hcy, homocysteine; NAC, N-acetylcysteine.

f, Effect of nutrient supplements on MR alone or with 5-FU -inhibited cell proliferation in CRC119 primary cells. Mean ± s.e.m., n=9 biologically independent samples from three independent experiments, * p<0.05 vs control, ^ p<0.05 vs MR, # p<0.05 vs 5-FU; $ p<0.05 vs MR+5-FU by two-tailed Student's t-test.

g, U-^{13}C-Serine tracing.

h, Mass intensity for M+1 dTTP and M+1 methionine in CRC119 cells. Mean ± s.d., n=3 biologically independent samples, *p<0.05 vs control, #p<0.05 vs MR by two-tailed Student's t-test.

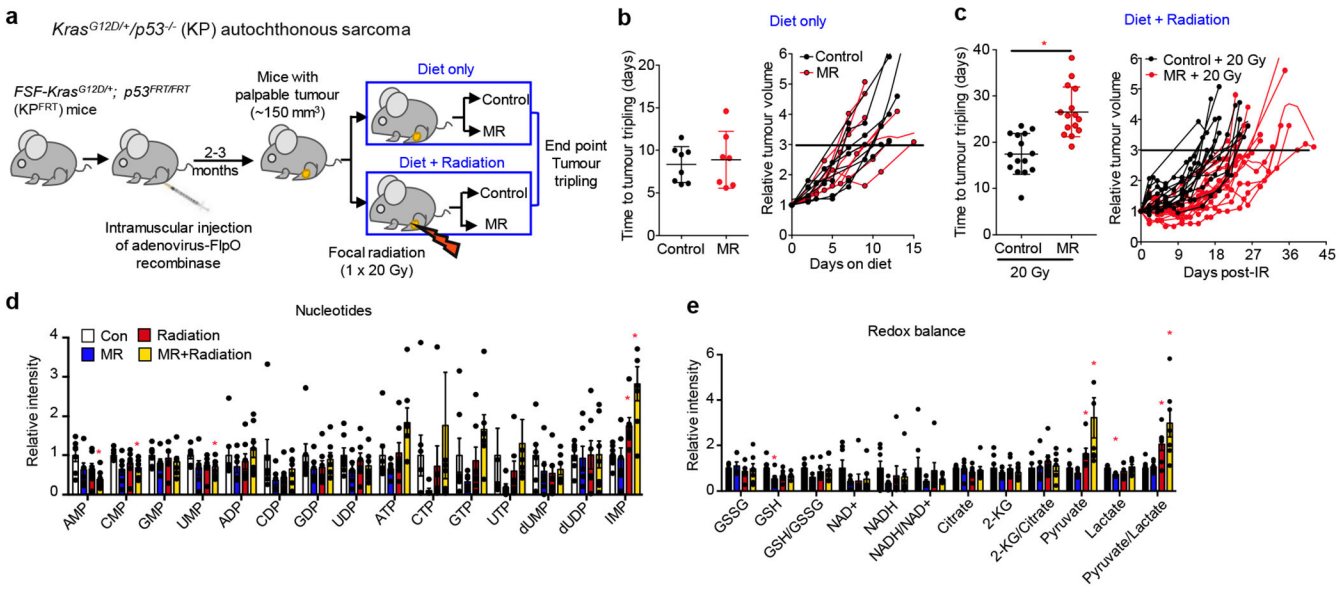

Fig. 3. Dietary MR sensitizes RAS-driven autochthonous sarcoma mouse models to radiation

a, Experimental design.

b, Time to tumour tripling and tumour growth curve from mice on dietary treatment only. Mean ± s.d., Control: n=8 animals, MR: n=7 animals.

c, Time to tumour tripling and tumour growth curve from mice on the combination of dietary treatment and radiation. Mean ± s.d., n=15 animals/group, *p<0.05 by two-tailed Student's t-test.

d-e, Relative intensity of nucleotides (d) and metabolites related to redox balance (e) in tumours. Mean ± s.e.m., n=7 animals/group except for MR (n=6), *p<0.05 compared to the control group by two-tailed Student's t-test.

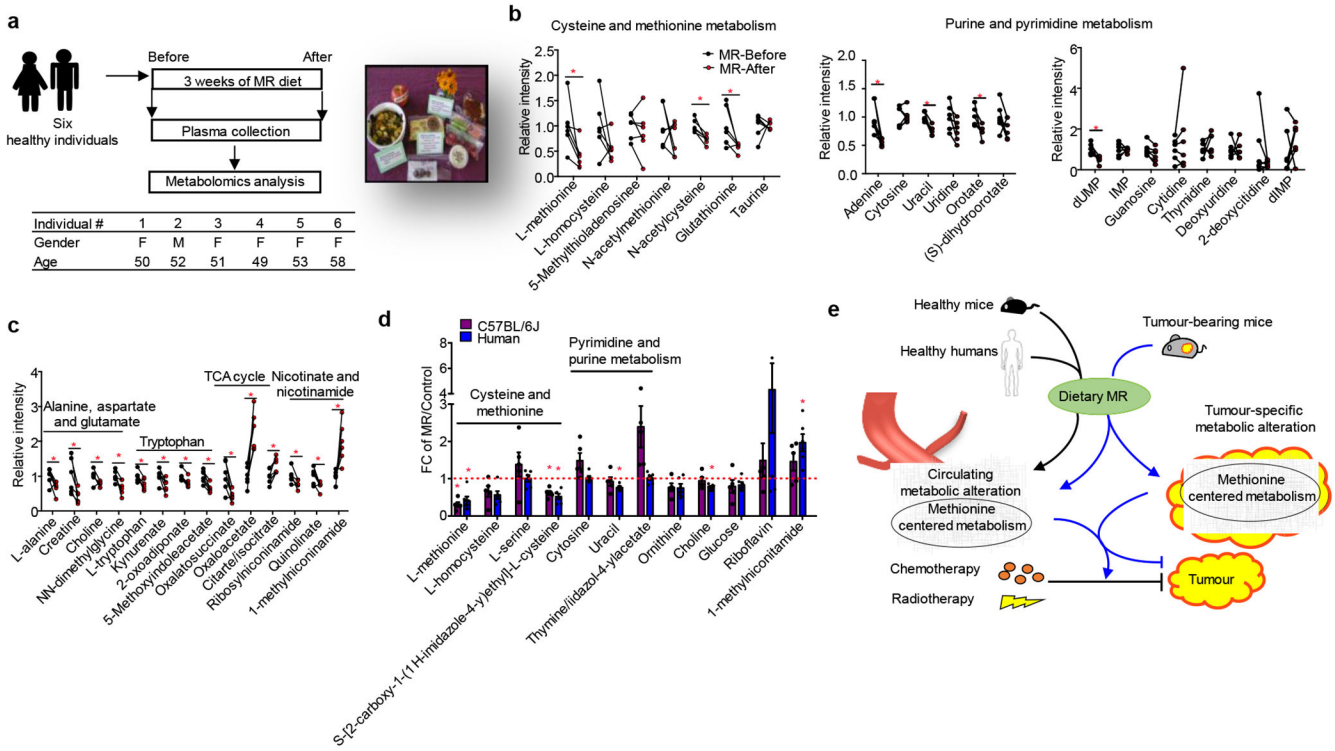

Fig. 4. Dietary MR can be achieved in humans

a, Experimental design, including background information on participated in the dietary study and representative daily MR diet.

b-c, Relative intensity of plasma metabolites related to cysteine and methionine metabolism, and purine and pyrimidine metabolism (b) and in the other top impacted pathways (c). N=6 humans, *p<0.05 by two-tailed Student's t-test.

d, MR-induced fold changes (FC) of plasma metabolites in cysteine and methionine metabolism, and pyrimidine and purine metabolism in C57BL/6J mice (n=5) and humans (n=6). Mean ± s.e.m., *p<0.05 by two-tailed Student's t-test.

e, Model